The removal efficiencies and mechanism of aniline degradation by peroxydisulfate activated with magnetic Fe-Mn oxides composite

Lin Qiao, Yu Shi, Qingli Cheng, Bingtao Liu and Jing Liu

ABSTRACT

The Fe-Mn oxides composite prepared by a chemical co-precipitation method was used as a heterogenous peroxydisulfate catalyst for the decomposition of aniline. This study investigated the mechanism of aniline degradation by PDS activated with catalyst. Reactive species resulting in the degradation of aniline was investigated via radical quenching experiments with different scavengers, including methanol, tert-butyl alcohol, EDTA and sodium azide. Based on the experiments made here, it is speculated that the predominant reactive species responsible for the degradation of aniline may be holes and singlet molecular oxygen rather than $SO_4^{\cdot-}$ and ·OH radicals. The degradation of compounds in catalyst/peroxydisulfate system was put forward. The three possible intermediates were speculated by high performance liquid chromatography-mass spectrometry, and two possible degradation pathways were proposed.

Key words | Fe-Mn oxides, intermediate, oxidation, peroxydisulfate, reaction mechanism

Lin Qiao
Yu Shi
Qingli Cheng
Bingtao Liu (corresponding author)
Jing Liu
School of Environment and Municipal Engineering,
North China University of Water Resources and Electric Power,
Zhengzhou, Henan 450011,
China
E-mail: *liubingtao@ncwu.edu.cn*

Qingli Cheng
Bingtao Liu
Henan Key Laboratory of water Environment Simulation and Treatment,
Zhengzhou, Henan, 450011,
China

HIGHLIGHTS

- Magnetic Fe-Mn particles based on spinel-type ferrite $MnFe_2O_4$ were synthesized.
- Diagrammatic sketch of aniline degradation mechanism by peroxydisulfate in the presence of $MnFe_2O_4$ system was demonstrated.
- Three main intermediate products and two possible paths were studied.

INTRODUCTION

As one of the most widely used sewage treatment technologies, advanced oxidation processes (AOPs) are applied in the oxidation of non-biodegradable, recalcitrant and toxic organic pollutants on account of the generation of highly reactive species under ambient conditions in recent years (Hodges *et al.* 2018). In previous studies, traditional AOPs based on the generation of hydroxyl radical (·OH), e.g. Fenton reaction (Fe^{2+}/H_2O_2) (Verma & Haritash 2019), electron-Fenton (Yong *et al.* 2017), UV/H_2O_2 (Benito *et al.* 2017), O_3/H_2O_2 (Can & Cakir 2010), have received popular attention owing to producing the strong oxidant ·OH (oxidation potential is 1.8–2.7 V vs. normal hydrogen electrode (NHE)) in mild reaction conditions. However, several weaknesses, such as narrow and limited pHs (2–4) under optimal conditions and the chemical instability and high-cost of hydrogen peroxide, were gradually discovered in the continuous research of the AOPs, leading to tremendously placed restrictions on its practical application (Duran *et al.* 2018; Huang *et al.* 2020).

In recent years, AOPs based on the generation of sulfate radical ($SO_4^{\cdot-}$) have been the focus of numerous studies, and

doi: 10.2166/wrd.2021.102

peroxymonosulfate (PMS, HSO_5^-) and peroxydisulfate (PDS, $S_2O_8^{2-}$) have been proposed as candidates for such a purpose (Wacławek *et al.* 2017). Compared with ·OH, sulfate radical ($SO_4^{\cdot-}$) not only carries forward the same advantages due to the higher reactive oxidation (2.5–3.1 V vs. NHE) (Zhu *et al.* 2019), but also solve the shortcomings resulting from its stability and wider working pH range (Hu & Long 2016). $SO_4^{\cdot-}$ is generated by activating the PDS and PMS through various methods such as heat (Ji *et al.* 2015), UV light (Khan *et al.* 2013), alkaline (Lominchar *et al.* 2018), metal ions (Wang *et al.* 2019a), and metal oxide (Du *et al.* 2017; Zhang *et al.* 2018) though the cleavage of their O–O bonds. They are both very stable in the solid state, but PDS is a cheaper oxidant than PMS (considered as oxone salt ($2KHSO_5{\cdot}KHSO_4{\cdot}K_2SO_4$) and H_2O_2 and have a higher oxidation potential than PMS (Zhou *et al.* 2019). Consequently, PDS has shown to be a promising application prospect for the decomposition of organic pollutants.

Among the catalytic methods in AOPs based on PDS, metal ion and metal oxide catalysis are gaining greater attention and have wider application rather than sonocatalysis, photocatalyst is and thermocatalysis because of the lower energy consumption and low price. Metal oxide can be reused and regenerated in the catalytic process, which demonstrates that metal oxide catalysis can further reduce the total cost compared with other methods (Zhou *et al.* 2019). In addition, the separation between catalysts and liquid in the waste water treated by the method is easy to be implemented in subsequent processes. Therefore, it is highly significant to research metal oxide catalysis in AOPs based on PDS.

Spinel-type ferrite oxides, mainly including $CuFe_2O_4$, $MgFe_2O_4$, $NiFe_2O_4$, $CoFe_2O_4$ and $MnFe_2O_4$ etc., have attracted attention due to their chemical stability and photochemical properties (Junlabhut *et al.* 2018). Recently, spinel-type ferrite oxides were used as the catalytic agent in AOPs. Wang *et al.* (2019b) report that 67% of levofloxacin was degraded within 1 h with the reaction condition of 0.6 g/L magnetic nickel ferrite/carbon sphere composite and 1.8 g/L PDS, which is described as a potentially useful catalyst in AOPs. Pan *et al.* (2017) reported that UV-filter benzophenone-3 in aqueous solution is removed in 6 h under the condition of $[\text{benzophenone-3}]_0$: $[PDS]_0 = 1{:}1{,}000$, catalyst load = 500 mg L^{-1}. Generally, spinel-type ferrite oxides have gained more attention in catalytic oxidation.

Although $SO_4^{\cdot-}$ is the main production of most persulfate processes, there are some investigations which indicate that partial persulfate activation processes involve a non-radical mechanism. Some investigations have found a non-radical mechanism for the degradation of organic contaminants. Zhang *et al.* (2014) reported that copper oxide (CuO) could efficiently activate PDS without producing $SO_4^{\cdot-}$. Meanwhile, Lee *et al.* (2015) reported that the persulfates bind onto the surface of CNTs, forming reactive complexes that are immediately decomposed upon reaction with organic compounds. Wu *et al.* (2018) discovered that the reaction of non-radical mechanism was observed in the degradation of aniline by rice straw biochar RSBC/PDS system and the holes were responsible for the reaction process. However, the research about the mechanism of non-radicals has not been greatly reported in current reports.

Single oxygen ($^1O_2$), which is one of the typical nonradical reactive oxygen species, has been widely used in the degradation of organic pollutants, particularly in photocatalytic degradation processes (Lee *et al.* 2011). The $^1O_2$ in the process of degradation has strong selectivity to organic pollutants owing to its electrophilic nature (Cheng *et al.* 2017). Some studies reported that the activation process of PDS can produce $^1O_2$ in some systems. Ma *et al.* (2018) reported that PDS is activated by nitrogen-doped mesoporous carbon to degrade the phenol through $^1O_2$ and electron transfer. Shi *et al.* (2020) reported that $^1O_2$ was one of the reactive oxidative species involved in the degradation of sulfamethoxazole through activation of persulfate by EDTA-2 K-derived nitrogen-doped porous carbons.

In this study, we investigated the activation mechanism of PDS by $MnFe_2O_4$ for the degradation of aniline. Radical scavengers identified the main reactive species responsible for aniline decomposed. Additionally, degradation mechanisms were proposed based on experimental results from spectroscopy measurement.

MATERIALS AND METHODS

Reagents and materials

All chemicals used in this study were at least of analytical grade and used as received without further purification,

except as noted. Aniline was provided by Sigma-Aldrich Chemical Co., Ltd (Shanghai, China). Potassium persulfate was provided by ANPEL Laboratory Technologies Reagent Inc. (Shanghai, China). N-(1-naphthyl) ethylenediamine dihydrochloride, iron (III) chloride hexahydrate ($FeCl_3 \cdot 6H_2O$) and manganese sulfate monohydrate ($FeSO_4 \cdot 6H_2O$) were supplied by Kermel Chemical Reagent (Tianjin, China). Methanol anhydrous (MeOH) and tert-Butanol (*t*-BuOH), serving the scavengers of radicals, were obtained from Macklin Biochemical Co., Ltd (Shanghai, China). Ethylenediaminetetraacetic acid disodium salt (EDTA-2Na) used as the hole scavenger and sodium azide (NaN_3) used as singlet molecular oxygen ($^1O_2$) scavenger, was bought from Guangfu Technology Development Co., Ltd (Chengdu, China). Deionized water was used throughout the experiments.

Synthesis of $MnFe_2O_4$

The $MnFe_2O_4$ catalyst was synthesized using the chemical coprecipitation method (Liu *et al.* 2020). First, 5.07 g $MnSO_4 \cdot H_2O$ and 16.5 g $FeCl_3 \cdot 6H_2O$ were dissolved into 300 mL deionized water (Mn^{2+}:$Fe^{3+} = 1$:2 at a molar ratio) with continuous mechanical stirring at 62°. Secondly, 8 M NaOH solution was added slowly to the mixture solution until the pH value of the solution reached approximately 11. Then, stirring was stopped and the mixture solution was maintained at 75° for 30 min. When cooling down to room temperature, the mixture solution was filtered to obtain the suspension which was then washed with deionized water and ethanol at least three times. Finally, the composite was calcined at 300° for 4 h in the muffle furnace and ground to powder for further use.

Characterization of $MnFe_2O_4$

The morphological representation and internal structure of $MnFe_2O_4$ was collected on a field emission scanning electron microscope (FE-SEM, JSM-6700F) equipped with energy-dispersive X-ray spectrometer and transmission electron microscopy (TEM, JEM-200CX, JEOL, Japan). Powder X-ray diffraction spectrum was recorded at 0.02°/s and operated at 40 kV and 15 mA current with Cu kα1 radiation ($\lambda =$ 0.15406 nm) diffractometer (XRD, Dmax 2,500 V). The various functional groups of $MnFe_2O_4$ were detected by Fourier-transform infrared (FTIR, Nicolet380).

Degradation experiments

In a typical run, conical flasks containing 50 mL reaction solution were kept at a controlled temperature in an air bath shaker (HNY-2102C, Honour, China) to conduct the tests. The initial concentration of aniline was 20 g/L. After 30 min of adsorption equilibrium between aniline and $MnFe_2O_4$, the oxidation reaction was initiated by adding a desired amount of PDS. The pH in the solution was adjusted by H_2SO_4 or NaOH solution. After 0, 30, 60, 90, 120, 180 and 240 min, respectively, 1 mL of reaction solution was withdrawn and filtered through a 0.45 mm membrane into a liquid sampling bottle for further analysis.

Analytical methods

The concentration of aniline was analyzed with the colorimetric method using N-(1-naphthyl) ethylenediamine as a chromogenic agent. An N5000 UV-VIS spectrometer (Shanghai Youke, China) was used to measure the absorbance in a 1 cm cell at 545 nm. The intermediates were identified on a Waters W2489-QDa (USA) high performance liquid chromatography (HPLC) equipped with a Waters QDa mass spectrometer with a reversed-phase C18 column (4.7 × 250 mm). The mobile phase was also the mixture of acetonitrile-water (55:45, *V:V*) and the flow rate was set at 0.50 mL/min. The mass spectrometer was operated under electrospray positive ionization at a fragmentor voltage of 800 V with a mass scan range of 50–600 amu. The ionization source conditions were set at the drying gas flow at 600 °C. The metal valance state was identified by X-ray photoelectron spectroscopy (XPS, Al Kα, AXIS Supra spectrometer, Shimadzu, Japan).

RESULTS AND DISCUSSION

Characterization of catalysts

The XRD patterns were used to analyze the information of material composition, structure or morphology of atoms or

molecules in materials. X-ray diffraction analysis is the main method to research the phase and crystal structure of materials. Thus, the X-ray diffraction of catalyst is shown in Figure 1 to determine the composition and crystallinity.

In the range of 2θ from 20 to 80°, it was noticed that there were several significant peaks in the X-ray diffraction of the material. The diffraction peaks at 2θ of 29.71, 34.98, 42.53, 56.20 and 61.66° mainly corresponded to the typical reflections of (220), (311), (400), (511) and (440) planes, respectively. The results mean that the material was indexed into the cubic spinel-type $MnFe_2O_4$ (JCPDS No. 38-0430). Wang *et al.* (2019b) also reported similar peaks in the XRD spectrum of $MnFe_2O_4$. Therefore, the pure $MnFe_2O_4$ was efficiently produced by using the chemical coprecipitation method in the experiment.

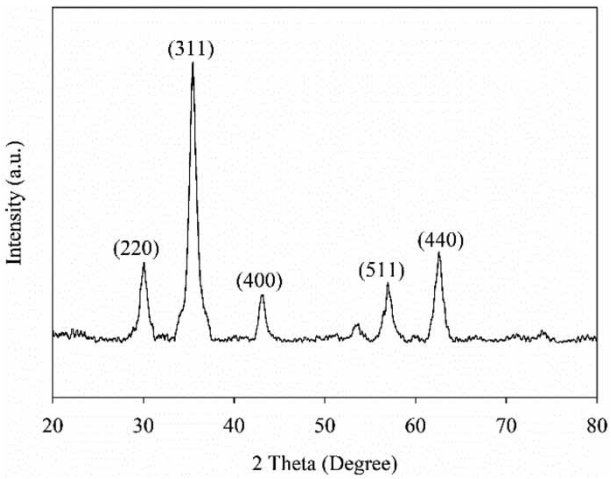

Figure 1 | XRD spectrum of $MnFe_2O_4$.

The transmission electron microscopy (TEM) and scanning electron microscope (SEM) images, where surface morphology and particle size was obtained, is demonstrated in Figure 2. It could be seen from TEM images that $MnFe_2O_4$ particles have spherical structures, while catalyst particles in micron scale with a diameter of 0.1–0.5 μm were confirmed by the SEM images.

The various functional groups of $MnFe_2O_4$ before and after reaction were confirmed in the FTIR spectra (Figure 3). The appearance of absorption peak at 3,424 cm^{-1} was due to the stretching vibrations of -OH moieties in carboxyl and hydroxyl groups (Yang *et al.* 2019). The corresponding functional groups with wave numbers of 2,853 and 2,923 cm^{-1}

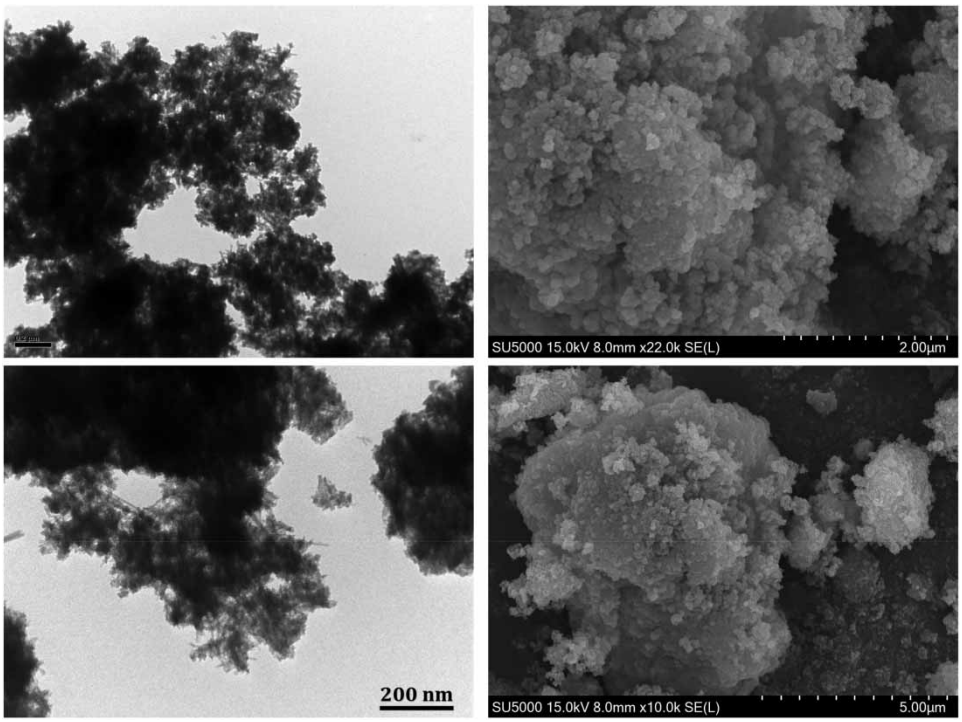

Figure 2 | SEM and TEM spectrum of $MnFe_2O_4$.

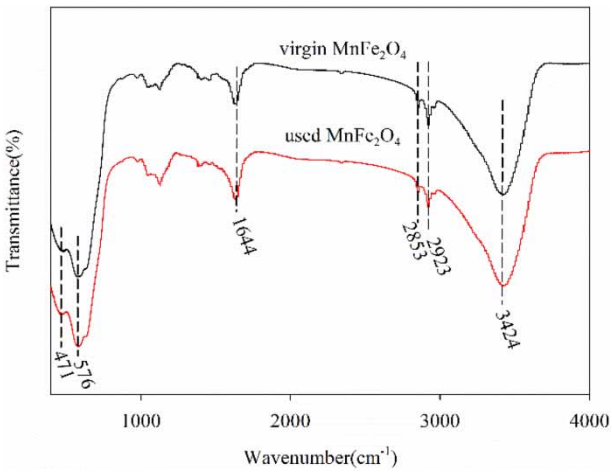

Figure 3 | FT-IR spectra of $MnFe_2O_4$.

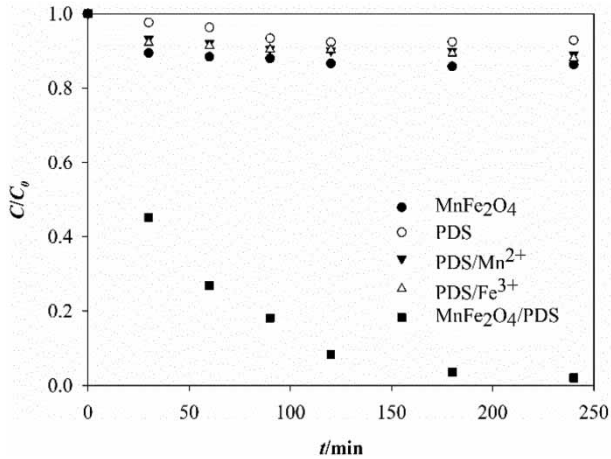

Figure 4 | Effect of different systems on degradation of aniline by PDS catalyzed with $MnFe_2O_4$. Experimental conditions: aniline = 20 mg/L, PDS = 2.4 mM, $MnFe_2O_4$ = 1.3 g/L, $Fe^{3+} = Mn^{2+}$ = 5.6 mM.

were associated to C-H stretching vibrations (Chakraborty *et al.* 2017). The peak at 1,644 cm^{-1} could be assigned to the bending vibrations of H_2O molecules on the surface of $MnFe_2O_4$ (Zhu *et al.* 2019). Furthermore, there were two strongly characteristic peaks in the wave numbers of 471 and 576 cm^{-1} which is related to Mn-O and Fe-O vibrations in $MnFe_2O_4$ respectively. The lower wave number of 471 cm^{-1} was assigned to the octahedral coordination Mn^{2+}, and the higher wave number of 576 cm^{-1} was related to the tetrahedral coordination Fe^{3+} (Kafshgari *et al.* 2017). It was observed that there were no differences in the FTIR spectra of the used and the virgin $MnFe_2O_4$. The results demonstrated the $MnFe_2O_4$ used as the catalyst was stable in the system $MnFe_2O_4$/PDS (Liu *et al.* 2020).

Degradation experiment in different systems

To confirm the $MnFe_2O_4$ accessed to activate PDS, Figure 4 shows the degradation of aniline by different systems. It can be seen that the maximum adsorption capacity of $MnFe_2O_4$ for aniline is 2.1 mg/L and aniline degradation by 2.4 mM PDS is only 7.1% at 240 min, which shows that they both had a negligible contribution to adsorb or oxidize the compound. Aniline removal efficiency in the $MnFe_2O_4$/PDS system was nearly 100% at 240 min. It is noteworthy that a pseudo-first-order degradation pattern ($R^2 > 0.90$) was suitable for the aniline removal in PDS activation by $MnFe_2O_4$ and the fitting reaction rate constant (k_{app}) was 0.016. Besides, aniline degradation efficiencies in PDS/Fe^{3+} and PDS/Mn^{2+} system was 11 and 12% at 240 min, respectively, demonstrating that the heterogeneous activation was the dominant oxidation in the $MnFe_2O_4$/PDS system. These results demonstrate that $MnFe_2O_4$ could effectively activate PDS. Similarly, Deng *et al.* (2017) reported that the degradation of bisphenol A by homogeneous Mn^{2+}/PMS, and Fe^{3+}/PMS activation was less than 10% compared with the degradation of 90% by $MnFe_2O_4$/PMS system. Abroshan *et al.* (2018) reported that $MnFe_2O_4$ had a certain function in catalyzing PDS for the removal of levofloxacin in aqueous solution.

Effect of initial pH and reaction temperture

The influence of initial pH ranging from 3.0 to 11.0 on aniline degradation is illustrated in Figure 5. It is clear that the aniline degradation in the $MnFe_2O_4$/PDS system showed high efficiencies over a wide pH range of 3.0–9.0 and strongly alkaline pH could not benefit the degradation of aniline. Specially, when the pH value increased from 3.0 to 9.0, the minimal removal efficiencies of aniline achieved 95% within 4 h, and the corresponding k_{obs} value was 0.0113 min^{-1}. The aniline degradation had a significant reduction with the increasing of initial pH value to 11 and the relevant k_{obs} was found to be 0.0019 min^{-1}. The pH_{pzc} of $MnFe_2O_4$, the pK_a of aniline, and the pH value of solution should all be taken into consideration when discussing the

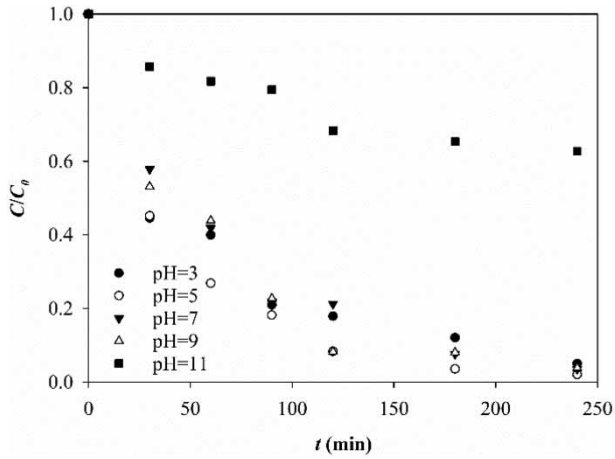

Figure 5 | Effect of solution initial pH on degradation of aniline by PDS catalyzed with $MnFe_2O_4$. Experimental conditions: initial pH = 5.00 ± 0.2 and T = 25°, initial concentration of aniline, PDS and $MnFe_2O_4$ were 20 mg/L, 2.4 mM, and 1.3 g/L, respectively.

influence of initial pH. It has been reported that the pK_a value of aniline is 4.6, which means that aniline exists mainly in cationic forms in solution at pH 3 and mainly as neutral in a pH range of 5–11. The pH_{pzc} of $MnFe_2O_4$ was determined to be 4.81. It demonstrated that the surface of the particle had a positive charge due to pH less than pH_{pzc} and would be negatively charged owing to pH larger than pH_{pzc}. To further determine the change of pH value in the system, variations of solution pH in these processes are also confirmed and it is clear that the values of pH from 30 to 240 min are controlled in a certain range from 4.50 to 3.50 when the initial pH was from 3.0 to 9.0 and the solution pH in 240 min tardily decreased to 10 when the initial pH was 11. Thus, as the initial pH value was under 10, the surface on $MnFe_2O_4$ would engender the electrostatic attraction force with PDS (anion) instead of the repulsion force with aniline. It could be speculated that the reaction between PDS and $MnFe_2O_4$ took precedence over the oxidative degradation of aniline in the PDS/$MnFe_2O_4$ system. As the initial pH value reached 11, the electrostatic attraction force between PDS and $MnFe_2O_4$ vanished ($pH > pH_{ZPC}$), leading to a decrease in the aniline degradation. Above all, it was likely that the $MnFe_2O_4$/PDS system had broad application prospects as part of wastewater treatment except in the strongly alkaline condition. What is more, to reach such prospects, the leaching of metal ion in this system is one of the questions of common interest. The leaching concentration of ferric ion after 4 h reaction was detected to be 0.14, 0.15, 0.1, 0.17 and 0.45 mg/L with the initial pH value increasing from 3.0 to 11.0 g/L, respectively. Meanwhile, the leaching concentration of manganese ion was 30.30,17.09, 13.40, 14.24 and 0.57 mg/L, respectively. The results show that further treatment in practical applications needs to be carried out for decreasing the concentration level of manganese in the solution.

The effect of reaction temperature in the $MnFe_2O_4$/PDS system was confirmed. Specially, the increasing of the corresponding k_{obs} values is from 0.0055 min^{-1} at 10 °C to 0.018 min^{-1} at 30 °C. The results showed reaction temperature is an essential factor for this system, thus it is hard for it to be widely used in some lower temperature areas.

Mechanism of aniline degradation by $MnFe_2O_4$/PDS systems

In terms of previous reports, the predominant reactive species in PDS activation were $SO_4^{\cdot-}$ and ·OH (Nie *et al.* 2014). It was reported that MeOH could quench both $SO_4^{\cdot-}$ ($k_{SO_4^{\cdot-}} = 1 \times 10^9\ M^{-1}\ s^{-1}$) and ·OH ($k_{\cdot OH} = 1 \times 10^7\ M^{-1}\ s^{-1}$). *t*-BuOH showed a high reaction rate in quenching ·OH ($k_{\cdot OH} = 5.2 \times 10^8\ M^{-1}\ s^{-1}$), yet it reacted slower with $SO_4^{\cdot-}$ ($k_{SO_4^{\cdot-}} = 8.4 \times 10^5\ M^{-1}\ s^{-1}$) than MeOH (Guan *et al.* 2018). Thus, MeOH and *t*-BuOH were used as scavengers to distinguish the existence of $SO_4^{\cdot-}$ and ·OH in $MnFe_2O_4$/PDS systems separately. As Figure 6 shows, the degradation of aniline by the $MnFe_2O_4$/PDS system was examined in the presence of excess radical scavengers. Both the introduction of MeOH and *t*-BuOH in PDS/$MnFe_2O_4$ system had little influence on the degradation of aniline even if the scavenger was 1,000 times the molar ratio of aniline. This suggested that the mechanism of $SO_4^{\cdot-}$ generation probably has little influence on the aniline decomposition by the $MnFe_2O_4$/PDS system. Similarly, Shi *et al.* (2020) reported that the removal rate of sulfamethoxazole through the PDS activated by EDTA-2 K-derived nitrogen-doped porous carbons only reduced by 23% as the addition of MeOH which demonstrated that $SO_4^{\cdot-}$ and ·OH were not dominantly responsible in the reaction system. However, $SO_4^{\cdot-}$ and ·OH were still generated in the system.

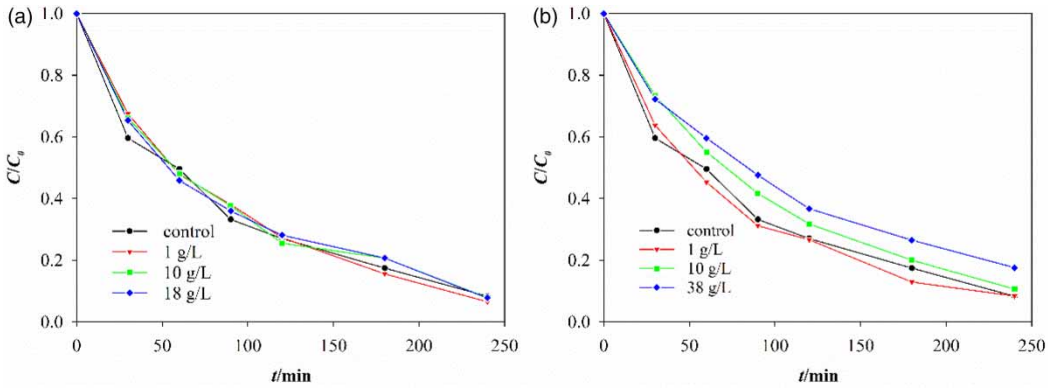

Figure 6 | Effect of different MeOH(a) and *t*-BuOH (b) on degradation of aniline by PDS catalyzed with $MnFe_2O_4$. Experimental conditions: initial concentration of aniline, PS and $MnFe_2O_4$ were 20 mg/L, 2.4 mM, and 0.9 g/L, respectively.

To verify whether the main reactive species in $MnFe_2O_4$/PDS system responsible for the degradation of aniline was the hole which was similar to photogenerated active sites, we tested the radical trapping experiments, where EDTA was added into the reaction system as the hole radical scavenger (Figure 7(a)). Specifically, the removal efficiencies of aniline after 4 h significantly decreased from 90.1 to 47.0% with the concentrate of EDTA increasing from 0.01 to 1.00 g/L, respectively. This result showed the possible involvement of the hole in the degradation of the aniline. However, Wu *et al.* (2018) reported that the degradation of aniline in RSBC/PDS was completely inhibited when the addition of EDTA reached 1.00 g/L. This demonstrated that the $MnFe_2O_4$/PDS system may produce other reactive species except holes.

One of the main photogenerated reactive species was $^1O_2$ (Zhang *et al.* 2020), which might have an effect on the facilitated degradation of aniline. To prove the hypothesis, NaN_3, which was used as the scavengers of $^1O_2$ to inhibit the oxidation process, was fed into the $MnFe_2O_4$/PDS system (Figure 7(b)). When the concentrate of NaN_3 increased to 1.00 g/L, the degradation of the aniline in the $MnFe_2O_4$/PDS system was drastically decreased to over half of the control system. This indicated that the generation of $^1O_2$ may be responsible for the degradation of aniline in the $MnFe_2O_4$/PDS system.

TOC removal efficiencies in $MnFe_2O_4$/PDS system

As shown in Figure 8, the removal efficiencies of TOC during the oxidation of aniline with different PDS concentrations were quantified. It can be seen that the TOC degradation degree of the PDS/$MnFe_2O_4$ system increased slowly with the reaction time. In particular, the TOC

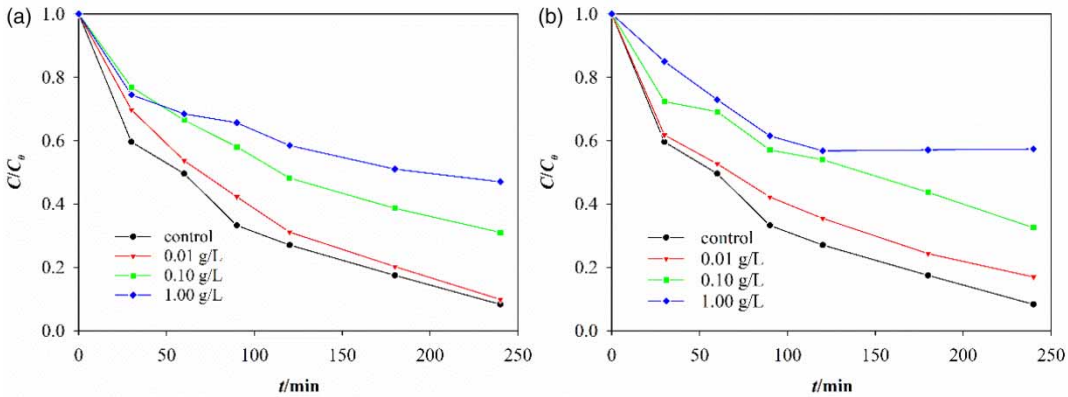

Figure 7 | Effect of different EDTA(a) and NaN_3 (b) concentration on degradation of aniline by PDS catalyzed with $MnFe_2O_4$. Experimental conditions: initial concentration of aniline, PS and $MnFe_2O_4$ were 20 mg/L, 2.4 mM, and 0.9 g/L, respectively.

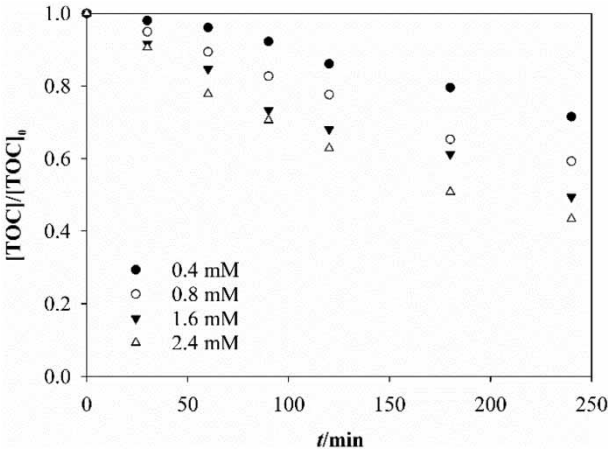

Figure 8 | Effect of different PDS concentrations on the removal efficiencies of TOC by PDS catalyzed with $MnFe_2O_4$. Experimental conditions: initial concentration of aniline and $MnFe_2O_4$ were 20 mg/L and 0.5 g/L, respectively.

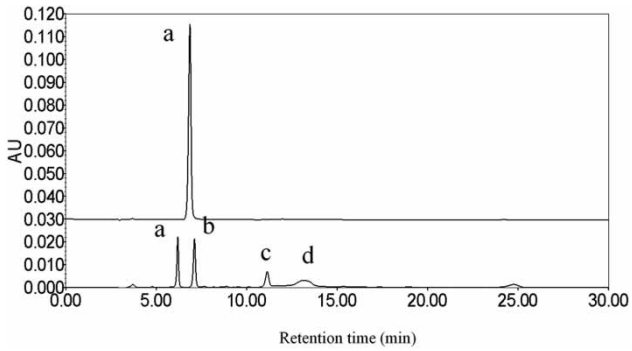

Figure 9 | HPLC typical chromatograms of intermediates (a–d) for aniline solutions collected after 0 and 4 h in MnFe2O4/PDS system.

removal efficiencies after 4 h were 71, 59, 49 and 43% for 0.4, 0.8, 1.6 and 2.4 mM PDS, respectively. These results indicated that some organic oxidation products were formed and remained in the reaction solution.

Identification of intermediates and transformation pathways

To further explore the mechanism of aniline degradation in the $MnFe_2O_4$/PDS system, high-performance liquid chromatography-mass spectrometry (HPLC-MS) was introduced to identify the intermediates during the $MnFe_2O_4$/PDS system. The detected samples collected at the reaction time of 0 and 4 h were extracted with n-Hexane (the extraction ratio was 1:1) to analyze in HPLC-MS (Xie *et al.* 2012), respectively. The three main intermediates in the system are shown in Figure 9. All the peaks in the chromatogram were marked to respond with the analytical results in mass spectrometry.

As shown in mass spectrometry (Figure 10), the peak of a, b, c and d corresponded to *m/z* values of 94.07, 201.16, 124.01 and 184.04, respectively. The chemical formulas of products in the system was proposed by both the mass spectrometry and the retention time. It can be observed that there are three main byproducts which have the chromatographic peak areas with *m/z* 201.16, 124.01 and 184.04.

Based on the above discussion, two possible degradation pathways of aniline degradation in the system were proposed and demonstrated in Figure 11. In pathway **I**, through the hydroxylation of aniline, the aromatic ring was first attacked by ·OH and $SO_4^{\cdot-}$ and the deprotonation of aniline accomplished, leading to the formation of imino radical. Next, imino radical was further oxidized by holes and $^1O_2$ into nitrobenzene. Then, a certain amount of nitrobenzene was possibly cleaved to small molecules such as the maleic acid and oxalic acid, and finally to CO_2. The other may react with imino radical resulting in converting into 4–4′-diaminodiphenyl, which was oxidized to small molecular organics by the reactive species. In pathway II, the intermediate dianiline resulting from the bimolecular reaction occurred. Further, the reactive species 'attacked', inducing benzene ring opening of dianiline to phenylsuccinic acid and maleic acid.

Through the analysis of XPS, which was carried out to elucidate the charge of chemical valence, the element composition of Mn and Fe species is further confirmed, see Figure 12. The C 1s peak was located at 284.8 eV in order to calibrate this spectrum (Figure 12(a)), and it was detected that the main chemical components including Fe, Mn and O continuously existed in $MnFe_2O_4$ during the reaction. Figure 12(b) showed that the two peaks locating at binding energy of 710 and 724 eV corresponded to Fe $2p_{3/2}$ and Fe $2p_{1/2}$ in spectrum of virgin $MnFe_2O_4$ (Lai *et al.* 2020), respectively, which strongly confirmed that only Fe(III) species existed in $MnFe_2O_4$ rather than the Fe(II). As shown in Figure 12(c), it can also be observed that the peaks centered at 641.8 eV (Mn $2p_{3/2}$) and 653 eV (Mn $2p_{1/2}$) suggesting that Mn(II) was the entire state of Mn species (Deng *et al.* 2018). After the

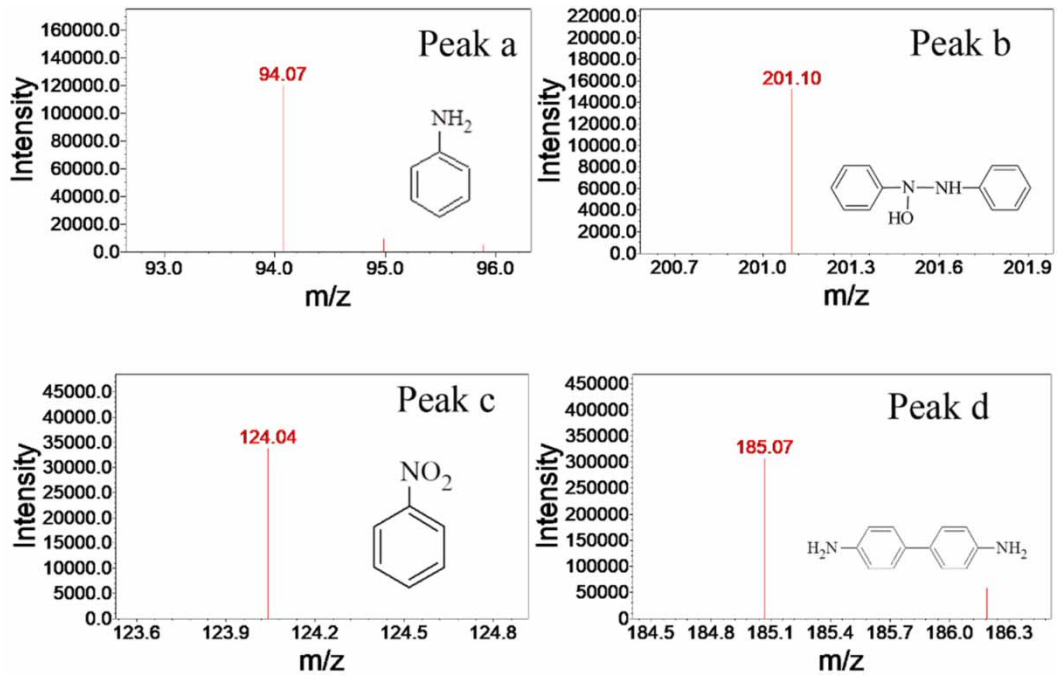

Figure 10 | Proposed intermediates and mass spectra of the degradation products.

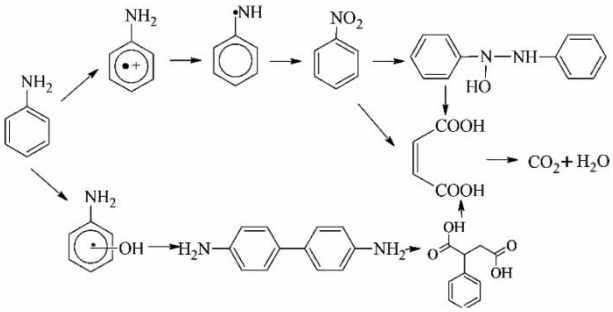

Figure 11 | Possible pathways of aniline mineralization by PDS/$MnFe_2O_4$.

reaction process, the peaks of Fe $2p_{3/2}$ located at 712.7 eV and Mn $2p_{3/2}$ located at 645.7 eV corresponded to Fe(II) and Mn(III), and deconvolution of these two peaks represents that multivalent states of Fe(II)/Fe(III) and Mn(II)/Mn(III) coexisted on the surface. The proportion of Fe(II)/(Fe(III) + Fe(II)) and Mn(II)/(Mn(III) + Mn(II)) increased to 33.02 and 51.57%, which confirmed that the chemical transformations between these multivalent states occurred on the surface of specimen. Figure 12(d) presented the O 1s spectrum of used and virgin $MnFe_2O_4$, which both had three peaks, one locating at 529.9 eV indicating the form of surface lattice oxygen (O_{latt}) and others locating at 531.7 and 533.2 eV derived from surface adsorbed oxygen (O_{ads},) (Lai *et al.* 2021). Due to its higher mobility than O_{latt}, O_{ads} could be integrated with Fe(III) and Mn(II) and then take part in the chain reaction in AOPs to the degradation of pollution (Kim & Shim 2010; Deng *et al.* 2017), and may cause the surface of $MnFe_2O_4$ to have more surface oxygen vacancies, which may further result in the generation of holes. Consequently, the proportion of O_{ads} in $MnFe_2O_4$ may affect the catalyst activity. Specially, the $MnFe_2O_4$ corresponding area ratio of $O_{ads}/(O_{ads} + O_{latt})$ was increased by 13.98% after the reaction, which demonstrated that the catalytic activity of $MnFe_2O_4$ after use was promoted to a certain extent.

According to the results above, a schematic diagram of the possible oxidation mechanism of aniline by PDS/$MnFe_2O_4$ is shown in Figure 13. It speculated that the degradation of compounds in the $MnFe_2O_4$/PDS system mainly contained three results: (1) the adsorption between the $S_2O_8^{2-}$ and the surface of $MnFe_2O_4$ occurred first; (2) then $S_2O_8^{2-}$ was converted by $MnFe_2O_4$ which was used as the electron donor into the production of not only holes and $^1O_2$ but also $SO_4^{\cdot-}$ and ·OH; (3) finally, reaction activation species reacted with compounds.

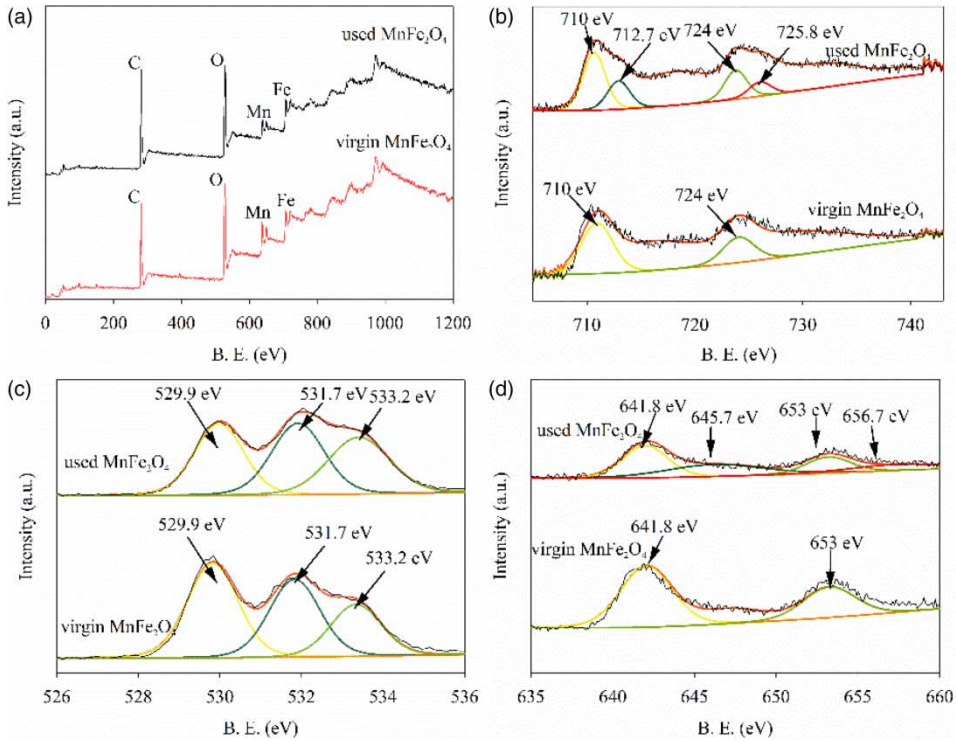

Figure 12 | XPS spectra of the virgin and used $MnFe_2O_4$: (a) full-range scan, (b) Fe 2p core level, (c) Mn core level O, and (d) 1 s core level.

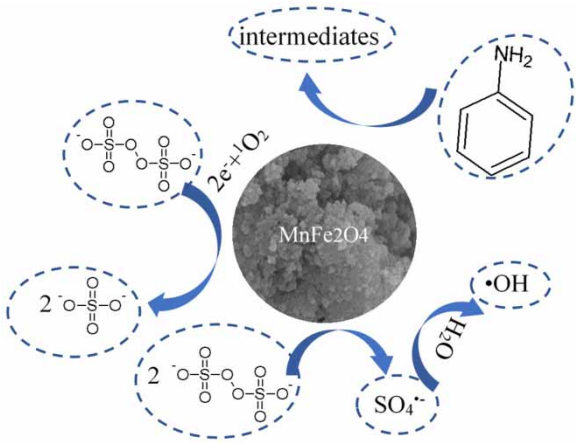

Figure 13 | Schematic diagram of the possible oxidation mechanism of aniline by PDS/$MnFe_2O_4$.

CONCLUSIONS

In this study, $MnFe_2O_4$ used as catalyst was synthesized by a chemical co-precipitation method and the heterogeneous catalytic oxidation of aniline with PDS was investigated; 97.98% of aniline was degraded in 4 h by $MnFe_2O_4$/PDS system. According to radical scavenging tests, both sulfate and hydroxyl radicals have little influence on the degradation of aniline in the $MnFe_2O_4$/PDS system. However, the degradation of aniline mainly depended on the reactive species of holes and $^1O_2$. There were several intermediate productions, including 4–4′-diaminodiphenyl, dianiline and nitrobenzene for the decomposition of aniline in the $MnFe_2O_4$/PDS system. All these productions were further broken into small molecular substances and finally into CO_2 and H_2O.

ACKNOWLEDGEMENTS

This work was financially supported by the Science and Technology Department of Henan (161100310700), and Key Research and Extension Project of Henan Province (192102310225).

DATA AVAILABILITY STATEMENT

Data cannot be made publicly available; readers should contact the corresponding author for details.

REFERENCES

Abroshan, E., Farhadi, S. & Zabardasti, A. 2018 Novel magnetically separable $Ag_3PO_4/MnFe_2O_4$ nanocomposite and its high photocatalytic degradation performance for organic dyes under solar-light irradiation. *Solar Energy Materials and Solar Cells* **178**, 154–163. doi:10.1016/j.solmat.2018.01.026.

Benito, A., Penades, A., Lliberia, J. L. & Gonzalez-Olmos, R. 2017 Degradation pathways of aniline in aqueous solutions during electro-oxidation with BDD electrodes and UV/H_2O_2 treatment. *Chemosphere* **166**, 230–237. doi:10.1016/j.chemosphere.2016.09.105.

Can, Z. S. & Cakir, E. 2010 Treatability of organic constituents in the pasakoy wastewater treatment plant effluent by O_3 and O_3/H_2O_2. *Ozone: Science & Engineering* **32** (3), 209–214. doi:10.1080/01919511003796087.

Chakraborty, I., Majumder, D., Talukdar, S., Roy, S. & Mandal, K. 2017 Surface engineered magneto fluorescent $MnFe_2O_4$ nanoparticles in the realm of biomedical applications. *Surfaces and Interfaces* **9**, 154–159. doi:10.1016/j.surfin.2017.09.005.

Cheng, X., Guo, H. G., Zhang, Y. L., Wu, X. & Liu, Y. 2017 Non-photochemical production of singlet oxygen via activation of persulfate by carbon nanotubes. *Water Research* **113**, 80–88. doi:10.1016/j.watres.2017.02.016.

Deng, J., Feng, S. F., Zhang, K. J., Li, J., Wang, H. Y., Zhang, T. Q. & Ma, X. Y. 2017 Heterogeneous activation of peroxymonosulfate using ordered mesoporous co3o4 for the degradation of chloramphenicol at neutral pH. *Chemical Engineering Journal* **308**, 505–515. doi:10.1016/j.cej.2016.09.075.

Deng, J., Xu, M., Qiu, C., Chen, Y., Ma, X., Gao, N. & Li, X. 2018 Magnetic $MnFe_2O_4$ activated peroxymonosulfate processes for degradation of bisphenol A: performance, mechanism and application feasibility. *Applied Surface Science* **459**, 138–147. doi:10.1016/j.apsusc.2018.07.198.

Du, X., Zhang, Y., Hussain, I., Huang, S. & Huang, W. 2017 Insight into reactive oxygen species in persulfate activation with copper oxide: activated persulfate and trace radicals. *Chemical Engineering Journal* **313**, 1023–1032. doi:10.1016/j.cej.2016.10.138.

Duran, A., Monteagudo, J. M., San Martin, I. & Merino, S. 2018 Photocatalytic degradation of aniline using an autonomous rotating drum reactor with both solar and UV-C artificial radiation. *Journal of Environmental Management* **210**, 122–130. doi:10.1016/j.jenvman.2018.01.012.

Guan, R., Yuan, X., Wu, Z., Wang, H., Jiang, L., Zhang, J., Li, Y., Zeng, G. & Mo, D. 2018 Accelerated tetracycline degradation by persulfate activated with heterogeneous magnetic $Ni_xFe_{3-x}O_4$ catalysts. *Chemical Engineering Journal* **350**, 573–584. doi:10.1016/j.cej.2018.05.195.

Hodges, B. C., Cates, E. L. & Kim, J. H. 2018 Challenges and prospects of advanced oxidation water treatment processes using catalytic nanomaterials. *Nature Nanotechnology* **13** (8), 642–650. doi:10.1038/s41565-018-0216-x.

Hu, P. & Long, M. 2016 Cobalt-catalyzed sulfate radical-based advanced oxidation: a review on heterogeneous catalysts and applications. *Applied Catalysis B: Environmental* **181**, 103–117. doi:10.1016/j.apcatb.2015.07.024.

Huang, D., Zhang, Q., Zhang, C., Wang, R., Deng, R., Luo, H., Li, T., Li, J., Chen, S. & Liu, C. 2020 Mn doped magnetic biochar as persulfate activator for the degradation of tetracycline. *Chemical Engineering Journal* **391**, 123532. doi:10.1016/j.cej.2019.123532.

Ji, Y., Dong, C., Kong, D., Lu, J. & Zhou, Q. 2015 Heat-activated persulfate oxidation of atrazine: implications for remediation of groundwater contaminated by herbicides. *Chemical Engineering Journal* **263**, 45–54.

Junlabhut, P., Nuthongkum, P. & Pechrapa, W. 2018 Influences of calcination temperature on structural properties of mnfe2o4 nanopowders synthesized by co-precipitation method for reusable absorbent materials. *Materials Today: Proceedings* **5** (6), 13857–13864. doi:10.1016/j.matpr.2018.02.028.

Kafshgari, L. A., Ghorbani, M. & Azizi, A. 2017 Fabrication and investigation of mnfe2o4/MWCNTs nanocomposite by hydrothermal technique and adsorption of cationic and anionic dyes. *Applied Surface Science* **419**, 70–83. doi:10.1016/j.apsusc.2017.05.019.

Khan, J. A., He, X., Khan, H. M., Shah, N. S. & Dionysiou, D. D. 2013 Oxidative degradation of atrazine in aqueous solution by UV/H_2O_2/Fe^{2+}, UV/$S_2O_8$2-/Fe^{2+} and UV/HSO_5-/Fe^{2+} processes: a comparative study. *Chemical Engineering Journal* **218**, 376–383. doi:10.1016/j.cej.2012.12.055.

Kim, S. C. & Shim, W. G. 2010 Catalytic combustion of VOCs over a series of manganese oxide catalysts. *Applied Catalysis B – Environmental* **98** (3–4), 180–185. doi:10.1016/j.apcatb.2010.05.027.

Lai, L. D., Zhou, H. Y., Zhang, H., Ao, Z. M., Pan, Z. C., Chen, Q. X., Xiong, Z. K., Yao, G. & Lai, B. 2020 Activation of peroxydisulfate by natural titanomagnetite for atrazine removal via free radicals and high-valent iron-oxo species. *Chemical Engineering Journal* **387**, 124165. doi:10.1016/j.cej.2020.124165.

Lai, L., Ji, H., Zhang, H., Liu, R., Zhou, C., Liu, W., Ao, Z., Li, N., Liu, C., Yao, G. & Lai, B. 2021 Activation of peroxydisulfate by V-Fe concentrate ore for enhanced degradation of carbamazepine: surface equivalent to V(III) and equivalent to V(IV) as electron donors promoted the regeneration of equivalent to Fe(II). *Applied Catalysis B – Environmental* **282**, 119559. doi:10.1016/j.apcatb.2020.119559.

Lee, J., Hong, S., Mackeyev, Y., Lee, C., Chung, E., Wilson, L. J., Kim, J. H. & Alvarez, P. J. J. 2011 Photosensitized oxidation of emerging organic pollutants by tetrakis C-60 aminofullerene-derivatized silica under visible light irradiation. *Environmental Science & Technology* **45** (24), 10598–10604. doi:10.1021/es2029944.

Lee, H., Lee, H. J., Jeong, J., Lee, J., Park, N. B. & Lee, C. 2015 Activation of persulfates by carbon nanotubes: oxidation of organic compounds by nonradical mechanism. *Chemical Engineering Journal* **266**, 28–33. doi:10.1016/j.cej.2014.12.065.

Liu, J., Qiao, L., Wang, Y., Li, G. & Liu, B. 2020 Aniline degradation by peroxydisulfate activated with magnetic Fe-Mn oxides composite: efficiency, stability, and mechanism. *Reaction Kinetics Mechanisms and Catalysis* **131** (2), 567–582. doi:10.1007/s11144-020-01861-1.

Lominchar, M. A., Santos, A., de Miguel, E. & Romero, A. 2018 Remediation of aged diesel contaminated soil by alkaline activated persulfate. *Science of the Total Environment* **622–623**, 41–48. doi:10.1016/j.scitotenv.2017.11.263.

Ma, W. J., Wang, N., Fan, Y. A., Tong, T. Z., Han, X. J. & Du, Y. C. 2018 Non-radical-dominated catalytic degradation of bisphenol A by ZIF-67 derived nitrogen-doped carbon nanotubes frameworks in the presence of peroxymonosulfate. *Chemical Engineering Journal* **336**, 721–731. doi:10.1016/j.cej.2017.11.164.

Nie, M., Yang, Y., Zhang, Z., Yan, C., Wang, X., Li, H. & Dong, W. 2014 Degradation of chloramphenicol by thermally activated persulfate in aqueous solution. *Chemical Engineering Journal* **246**, 373–382.

Pan, X., Yan, L., Li, C., Qu, R. & Wang, Z. 2017 Degradation of UV-filter benzophenone-3 in aqueous solution using persulfate catalyzed by cobalt ferrite. *Chemical Engineering Journal* **326**, 1197–1209. doi:10.1016/j.cej.2017.06.068.

Shi, Y. W., Zhu, J. D., Yuan, G., Liu, G. Z., Wang, Q. F., Sun, W. J., Zhao, B., Wang, L. & Zhang, H. W. 2020 Activation of persulfate by EDTA-2 K-derived nitrogen-doped porous carbons for organic contaminant removal: radical and non-radical pathways. *Chemical Engineering Journal* **386**, 124009. doi:10.1016/j.cej.2019.124009.

Verma, M. & Haritash, A. K. 2019 Degradation of amoxicillin by Fenton and Fenton-integrated hybrid oxidation processes. *Journal of Environmental Chemical Engineering* **7** (1), 102886. doi:10.1016/j.jece.2019,102886.

Wacławek, S., Lutze, H. V., Grübel, K., Padil, V. V. T., Černík, M. & Dionysiou, D. D. 2017 Chemistry of persulfates in water and wastewater treatment: a review. *Chemical Engineering Journal* **330**, 44–62. doi:10.1016/j.cej.2017.07.132.

Wang, S., Wu, J., Lu, X., Xu, W., Gong, Q., Ding, J., Dan, B. & Xie, P. 2019a Removal of acetaminophen in the Fe^{2+}/persulfate system: kinetic model and degradation pathways. *Chemical Engineering Journal* **358**, 1091–1100. doi:10.1016/j.cej.2018.09.145.

Wang, Z. J., Zhang, X. Y., Zhang, H. X., Zhu, G. X., Gao, Y. J., Cheng, Q. F. & Cheng, X. W. 2019b Synthesis of magnetic nickel ferrite/carbon sphere composite for levofloxacin elimination by activation of persulfate. *Separation and Purification Technology* **215**, 528–539. doi:10.1016/j.seppur.2019.01.063.

Wu, Y., Guo, J., Han, Y., Zhu, J., Zhou, L. & Lan, Y. 2018 Insights into the mechanism of persulfate activated by rice straw biochar for the degradation of aniline. *Chemosphere* **200**, 373–379. doi:10.1016/j.chemosphere.2018.02.110.

Xie, X., Zhang, Y., Huang, W. & Huang, S. 2012 Degradation kinetics and mechanism of aniline by heat-assisted persulfate oxidation. *Journal of Environmental Sciences* **24** (5), 821–826. doi:10.1016/s1001-0742(11)60844-9.

Yang, W. C., Jiang, Z., Hu, X. X., Li, X. Y., Wang, H. Y. & Xiao, R. Y. 2019 Enhanced activation of persulfate by nitric acid/annealing modified multi-walled carbon nanotubes via non-radical process. *Chemosphere* **220**, 514–522. doi:10.1016/j.chemosphere.2018.12.136.

Yong, X. Y., Gu, D. Y., Wu, Y. D., Yan, Z. Y., Zhou, J., Wu, X. Y., Wei, P., Jia, H. H., Zheng, T. & Yong, Y. C. 2017 Bio-Electron-Fenton (BEF) process driven by microbial fuel cells for triphenyltin chloride (TPTC) degradation. *Journal of Hazardous Materials* **324**, 178–183. doi:10.1016/j.jhazmat.2016.10.047.

Zhang, T., Chen, Y., Wang, Y., Le Roux, J., Yang, Y. & Croue, J. P. 2014 Efficient peroxydisulfate activation process not relying on sulfate radical generation for water pollutant degradation. *Environmental Science & Technology* **48** (10), 5868–5875. doi:10.1021/es501218f.

Zhang, Y., Zhang, Q., Dong, Z., Wu, L. & Hong, J. 2018 Degradation of acetaminophen with ferrous/copperoxide activate persulfate: synergism of iron and copper. *Water Research* **146**, 232–243. doi:10.1016/j.watres.2018.09.028.

Zhang, B. T., Wang, Q., Zhang, Y., Teng, Y. G. & Fan, M. H. 2020 Degradation of ibuprofen in the carbon dots/Fe_3O_4 carbon sphere pomegranate-like composites activated persulfate system. *Separation and Purification Technology* **242**, 116820. doi:10.1016/j.seppur.2020.116820.

Zhou, Z., Liu, X. T., Sun, K., Lin, C. Y., Ma, J., He, M. C. & Ouyang, W. 2019 Persulfate-based advanced oxidation processes (AOPs) for organic-contaminated soil remediation: a review. *Chemical Engineering Journal* **372**, 836–851. doi:10.1016/j.cej.2019.04.213.

Zhu, J., Chen, C., Li, Y., Zhou, L. & Lan, Y. 2019 Rapid degradation of aniline by peroxydisulfate activated with copper-nickel binary oxysulfide. *Separation and Purification Technology* **209**, 1007–1015. doi:10.1016/j.seppur.2018.09.055.

First received 31 October 2020; accepted in revised form 20 January 2021. Available online 11 March 2021